Quantum criticality at the boundary of the non-Hermitian regime of a Floquet system

Wen-Lei Zhao [1,*] and Jie Liu [2,3,†]

[1]*School of Science, Jiangxi University of Science and Technology, Ganzhou 341000, China*

[2]*Graduate School of China Academy of Engineering Physics, Beijing 100193, China*

[3]*CAPT, HEDPS, and IFSA Collaborative Innovation Center of the Ministry of Education, Peking University, Beijing 100871, China*

(Received 4 July 2023; accepted 30 April 2024; published 13 May 2024)

We investigate both analytically and numerically the dynamics of quantum scrambling, characterized by out-of-time ordered correlators (OTOCs), in a non-Hermitian quantum kicked rotor subject to quantum resonance conditions. Analytical expressions for OTOCs as a function of time are obtained, demonstrating a sudden transition from linear growth to quadratic growth when the non-Hermitian parameter decays to zero. At this critical point, the rates of the linear growth are found to diverge to infinity, indicating the existence of quantum criticality at the boundary of the non-Hermitian regime. The underlying mechanism of this quantum criticality is uncovered, and possible applications in quantum metrology are discussed.

DOI: 10.1103/PhysRevA.109.052215

I. INTRODUCTION

Uncovering new phases and determining the scaling laws of phase transitions at critical points are of interest in physics [1]. Quantum criticality, characterized by nonanalytical behavior of observables, arises from the singularity of an energy band landscape [2]. For instance, Dirac points cause the quantized growth of conductance in electron gases as the magnetic field varies [3]. In Floquet systems, critical behavior is determined by the singularity of quasienergy bands [4–8]. It is found that the saddle points in the quasienergy landscape lead to a logarithmic divergence in the density of states, akin to excited-state phase transitions in static systems, resulting in a magnetization cusp [9–11]. Quantum criticality is rooted in the emergence of large quantum fluctuations and long-range correlations [1,12,13], whose spatiotemporal propagation can be well quantified by out-of-time ordered correlators (OTOCs) [14,15]. Indeed, both theoretical and experimental investigations demonstrate that OTOCs can be used as order parameters to detect equilibrium [16–18], dynamical [19–21], and topological phase transitions [22,23].

Non-Hermiticity is an essential feature of different systems [24,25], including cold atoms [26,27], optics [28–30], and dissipative systems [31–33]. Non-Hermitian degeneracies in absorbing anisotropic crystals determine the transmission of polarized light [34–36]. Non-Hermitian random matrix theory is employed to describe the spontaneous breaking of chiral symmetry in quantum chromodynamics [37,38]. Both experimental and theoretical investigations have unveiled fundamental concepts, such as the non-Bloch bulk-boundary correspondence in topological phases [39], non-Hermitian skin effects [40–42], and nonreciprocal Landau-Zener tunneling [43]. The quantum critical phenomenon in non-Hermitian systems is still an elusive issue and has attracted increasing interest recently. Interestingly, the dynamics of OTOCs is governed by the Yang-Lee edge singularity [44] and spontaneous $\mathcal{PT}$-symmetry breaking [45,46]. Notably, OTOCs exhibit a quantized phenomenon in $\mathcal{PT}$-symmetric Floquet systems, indicating the emergence of a novel phase [47].

In this paper, we investigate the quantum critical phenomenon, quantified by OTOCs, via a non-Hermitian quantum kicked rotor (NQKR) model with complex kicking strength. We analytically obtain the time dependence of various OTOCs under the quantum resonance condition, revealing their linear growth over time for non-Hermitian kicking. In the Hermitian case, the OTOCs may increase quadratically or remain constant, depending on their specific form. Thus, there exists a sudden transition in the dynamics of the OTOCs at the boundary of the non-Hermitian regime. Interestingly, the growth rate of the OTOCs diverges towards infinity as the non-Hermitian parameter decays to zero, providing evidence of the presence of quantum critical behavior. The finding of quantum criticality at the boundary of the non-Hermitian regime has important implications for the foundation of the non-Hermitian extension of quantum physics. Our results suggest that the OTOCs can be used to identify the nonequilibrium dynamical signatures of quantum phase transitions in non-Hermitian Floquet systems [48–50].

The paper is organized as follows. In Sec. II, we describe the NQKR model and show the quantum critical behavior of OTOCs. Section III contains a theoretical analysis of the dynamics of OTOCs. The conclusion and discussion are presented in Sec. IV.

II. MODEL AND MAIN RESULTS

The dimensionless Hamiltonian of the NQKR model reads

$$\mathrm{H} = \frac{p^2}{2} + V_K(\theta)\sum_n \delta(t - t_n), \tag{1}$$

*wlzhao@jxust.edu.cn

†jliu@gscaep.ac.cn

with the complex kicking potential

$$V_K(\theta) = (K + i\lambda)\cos(\theta), \tag{2}$$

where $p = -i\hbar_{\rm eff}\partial/\partial\theta$ is the angular momentum operator, and θ is the angle coordinate, satisfying the commutation relation $[\theta, p] = i\hbar_{\rm eff}$, with $\hbar_{\rm eff}$ an effective Planck constant. Here, the parameters K and λ control the strength of the real and imaginary parts of the kicking potential, respectively [51,52]. The complex potential is realizable in the atom-optics experiments [53]. Ultracold atoms have a ground state E_1, excited states with two hyperfine levels $E_2^{\pm}$, and a noninteracting state E_i. The frequency of resonance laser satisfies the condition $(E_2^+ - E_1)/\hbar$, inducing effectively the transition from E_1 to E_2^+. This facilitates the decay from the excited state E_2^+ to a noninteracting energy level E_i, resulting in a loss of particle numbers that mimics the imaginary component of the potential. On the other hand, a far-tuned standing light wave generates a dipole force on the atoms and effectively plays the role of the real component of the complex potential. Moreover, the relative phase between the off-resonance and resonance standing waves can be precisely adjusted [26].

The eigenequation of the angular momentum operator is $p|n\rangle = p_n|n\rangle$ with eigenvalue $p_n = n\hbar_{\rm eff}$ and eigenstate $\langle\theta|n\rangle = e^{in\theta}/\sqrt{2\pi}$. With this complete basis, an arbitrary state can be expanded as $|\psi\rangle = \sum_n \psi_n|n\rangle$. The advancement of the δ-kicking potential is that the corresponding Floquet operator can be split into two components, namely $U = U_f U_K$, with the free evolution operator $U_f = \exp(-ip^2/2\hbar_{\rm eff})$ and the kicking term $U_K = \exp[-iV_K(\theta)/\hbar_{\rm eff}]$. The time evolution of a quantum state from t_n to t_{n+1} is governed by $|\psi(t_{n+1})\rangle = U|\psi(t_n)\rangle$.

The OTOCs are defined as $C(t) = -\langle[A(t), B]^2\rangle$, where both $A(t) = U^\dagger(t)AU(t)$ and B are operators evaluated in a Heisenberg picture, and $\langle\cdot\rangle = \langle\psi(t_0)|\cdot|\psi(t_0)\rangle$ is the expectation value of the operator with respect to the initial state [54–58]. Some specific operators have been exploited in the expression of OTOCs, and the growth rates of these OTOCs can be used to quantify the quantum chaos, thermalization, and entanglement [47,59–61]. In the first case, we consider the combination of a unitary operator $A = e^{i\varepsilon p}$ and a projection operator $B = |\psi(t_0)\rangle\langle\psi(t_0)|$, which results in the OTOCs $C_f = 1 - |\langle\psi(t)|e^{i\varepsilon p}|\psi(t)\rangle|^2$. In the second case, we utilize the operators $A = p$ and $B = \theta$, yielding $C_p = -\langle[p(t), \theta]^2\rangle$.

The C_f is closely related to some important physical quantities, such as the Frobenius norm and quantum Fisher information (QFI). Specifically, the Frobenius norm is constructed by the Fourier spectrum of C_f and has practical applications in measuring multiple quantum coherence [62]. Moreover, the second moment of the Frobenius norm provides a lower bound on the QFI [62]. If we choose the angular momentum operator as a generator of QFI, it is proportionally related to the mean energy [63,64]. For the C_p, the squared commutator between the angular momentum and the angle coordinate at different times diagnoses how the action of the angular momentum operator on the quantum state at a given time t affects the measurement of the angle coordinate at the end of time reversal, i.e., $t = t_0$. The semiclassical approximation of C_p, i.e., $C_p \approx \hbar_{\rm eff}^2\langle[\partial p(t)/\partial\theta(t_0)]^2\rangle_{\rm cl}$, with $\langle\cdots\rangle_{\rm cl}$ indicating the average over an ensemble of classical trajectories, can effectively quantify the exponentially fast departure of nearby trajectories in phase space due to chaotic instability [65,66]. In this context, we adopt these two OTOCs to investigate the genuine non-Hermitian dynamics in our system.

Quantum resonance arises from the requirement that each element of the free evolution operator matrix is unity, i.e., $U_f(n) = \exp(-in^2\hbar_{\rm eff}/2) = 1$, leading to the condition $\hbar_{\rm eff} = 4\pi$. We focus solely on the condition of quantum resonance $\hbar_{\rm eff} = 4\pi$. Our main findings can be summarized by the following relationships:

$$C_f \approx \begin{cases} \frac{2\pi\varepsilon^2(K^2+\lambda^2)}{\lambda}t & \text{for} \quad \lambda > 0, t \gg 1/\lambda, \\ \frac{\varepsilon^2K^2t^2}{2} & \text{for} \quad \lambda = 0 \end{cases} \tag{3}$$

and

$$C_p \approx \begin{cases} \frac{2\pi^3(K^2+\lambda^2)}{\lambda}t & \text{for} \quad \lambda > 0, t \gg 1/\lambda, \\ 16\pi^2 & \text{for} \quad \lambda = 0. \end{cases} \tag{4}$$

These relations clearly demonstrate the non-Hermiticity-induced linear increase of both $C_f(t)$ and $C_p(t)$ with time. Notably, the growth rates $G_f = dC_f/dt$ and $G_p = dC_p/dt$ take the form

$$G_{f,p} \approx \begin{cases} \frac{2\pi\varepsilon^2(K^2+\lambda^2)}{\lambda} & \text{for} \quad C_f, \\ \frac{2\pi^3(K^2+\lambda^2)}{\lambda} & \text{for} \quad C_p, \end{cases} \tag{5}$$

which display the remarkable divergence of both G_f and G_p as λ approaches zero, indicating the emergence of an abrupt transition at the non-Hermitian boundary.

To verify the theoretical predictions mentioned above, we numerically investigate the time dependence for both C_f and C_p over a wide range of λ. It is worth noting that our system does not possess well-defined thermal states, as the temperature of periodically driven systems tends to increase infinitely over time [67]. Consequently, there is no need to perform thermal averaging when calculating the OTOCs. Without loss of generality, we select the ground state of the angular momentum operator as the initial state in numerical simulations, i.e., $\psi(t_0) = 1/\sqrt{2\pi}$. Figure 1(a) shows that C_f increases in the quadratic function of time for the Hermitian case, i.e., $\lambda = 0$. For small values of λ, i.e., $0 < \lambda \ll 1$, C_f undergoes quadratic growth with respect to $\lambda = 0$ for a finite time interval $t < t_c$, after which it transitions to linear growth (see Fig. 2). The critical time t_c at which this transition occurs follows an inverse relationship with λ, i.e., $t_c \propto 1/\lambda$. Interestingly, for sufficiently large λ [e.g., $\lambda = 1$ in Fig. 1(a)], C_f exhibits a linear growth. Both the linear and quadratic behaviors are in perfect agreement with our theoretical predictions in Eq. (3). We further investigate the growth rate G_f of C_f for different λ. Figure 1(b) illustrates that, for a specific K (e.g., $K = 5$), the G_f initially decreases monotonically to a minimum value with the increase of λ, and then it increases. This behavior of G_f is in good agreement with our theoretical prediction in Eq. (5), which suggests a divergence of G_f as λ approaches zero. For $\lambda = 0$, the C_p remains constant over time, while for sufficiently large λ [e.g., $\lambda = 1$ in Fig. 1(c)], it linearly increases with time, in accordance with the laws described in Eq. (4). The corresponding growth G_p demonstrates the divergence of G_p with $\lambda \to 0$, confirming the validity of the theoretical prediction in Eq. (5) [see Fig. 1(d)].

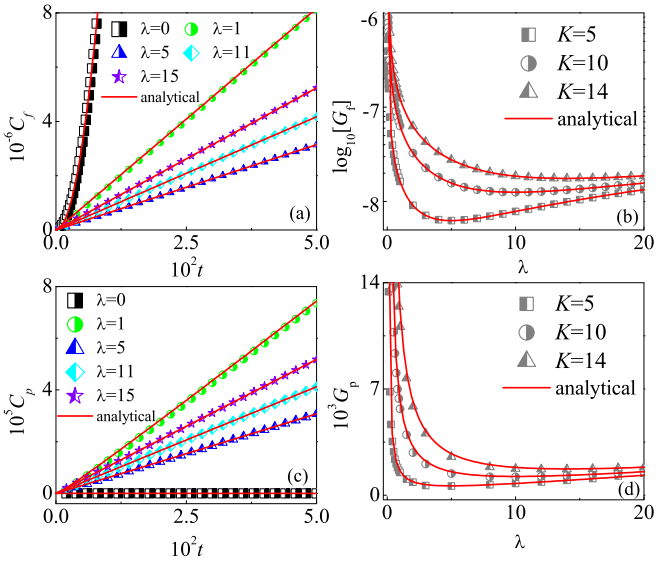

FIG. 1. Left panels: Time dependence of C_f (a) and C_p (c) with $K = 5$ for $\lambda = 0$ (squares), 1 (circles), 5 (triangles), 11 (diamonds), and 15 (pentagram). In (a) and (c), red lines indicate the theoretical prediction in Eqs. (3) and (4), respectively. Right panels: The growth rate G_f (b) and G_p (d) vs λ for $K = 5$ (squares), 10 (circles), and 14 (triangles). In (b) and (d), red lines separately indicate the theoretical prediction in Eq. (5). The parameters are $\hbar_{\text{eff}} = 4\pi$ and $\varepsilon = 10^{-5}$.

Our above investigation indicates that the non-Hermitian effects make C_f grow slower and C_p grow faster. Interestingly, for nonzero λ, we find that both C_f and C_p grow linearly with time even under the quantum resonance condition. Note that C_f is proportional to the mean energy, as will be shown in the next section. It is known that, in the Hermitian case, i.e., $\lambda = 0$, the mean energy diffuses ballistically with time

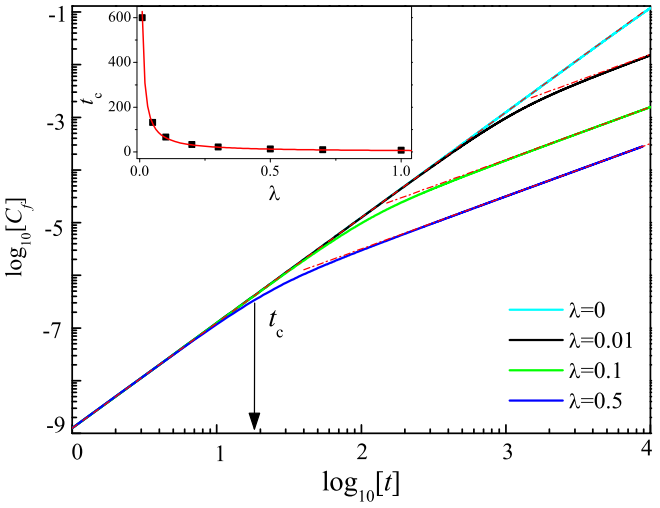

FIG. 2. (In logarithmic scale) C_f vs time for $\lambda = 0$ (cyan line), 0.01 (black line), 0.1 (green line), and 0.5 (blue line). The arrow marks the critical time t_c. Dashed and dash-dotted lines indicate our theoretical predictions $C_f \approx \varepsilon^2 K^2 t^2/2$ and $C_f \approx 2\pi\varepsilon^2(K^2 + \lambda^2)t/\lambda$ [see Eq. (3)], respectively. Inset: The critical time t_c vs λ. The red line indicates the inverse law $t_c \propto 1/\lambda$. The parameters are $K = 5$, $\varepsilon = 10^{-5}$, and $\hbar_{\text{eff}} = 4\pi$.

$\propto t^2$ [68], hence leading to the quadratic growth of C_f. For a nonzero value of λ, the non-Hermiticity suppresses the ballistic energy diffusion, resulting in the slower linear growth of C_f. For $\lambda = 0$, the cancellation between the two-point correlators and the four-point correlators results in the constant of C_p. In the non-Hermitian case, the contribution of the two-point correlators dominates the faster linear growth of C_p.

As is well known, in the traditional Hermitian kicked rotor system, for the nonresonance case where the quantum-coherence-induced dynamical localization emerges, external noises might destroy the quantum correlation and lead to the linear growth of mean energy (being proportional to C_f) [69]. In this situation, the quantum system will tend to revert back to classical uncorrelated diffusion [70]. For the resonance case, the small noises, however, cannot alter the ballistic energy diffusion because this situation lacks a classical counterpart in the limit in which the Planck constant tends to be zero [68]. Nevertheless, there is a fictitious classical limit in which the detuning ϵ of the driving period from the resonance condition plays the role of the effective Planck constant [71]. Robustness against noise is expected, due to the ϵ-classical nature of the dynamics [71]. The breakdown of the ballistic energy diffusion due to the non-Hermiticity unambiguously indicates that the NQKR cannot be simply equivalent to the standard kicked rotor with some kinds of noises induced by particle gain or loss. Thus, the changes of both C_f and C_p to the usual linear growth should be ascribed to non-Hermiticity rather than simple destruction of correlations by noise.

The presence of a new phase is clearly indicated by the distinct linear growth of OTOCs with time, where the growth rates, i.e., G_f and G_p in Eq. (5), exhibit a nonanalytical transition at $\lambda = 0$. This suggests that both G_f and G_p can serve as order parameters defining the phase with a quantum criticality during the abrupt transition at the boundary of the non-Hermitian regime. Note that the threshold value of the non-Hermitian parameter, determined by the appearance of complex quasienergies, is usually not identical to the mathematical boundary of the non-Hermitian regime [45,50,72,73], while recently, in a $\mathcal{PT}$-symmetric kicked rotor model under the quantum resonance condition, it was found numerically that the complex quasienergies emerge exactly at the boundary of the non-Hermitian regime [74]. Our analytical deduction explicitly demonstrates that this holds true for a general non-Hermitian Floquet system under the quantum resonance condition, and the underlying quantum critical phenomenon can be well depicted by the behaviors of the time evolution of the OTOCs at the non-Hermitian boundary. The non-Hermitian extension of the kicked rotor model is motivated by experimental realizations of this system with an all-optical setup, where the light transport in lossy media is governed by the non-Hermitian potential [74]. In fact, non-Hermitian physics has been recognized as a significant modification to conventional quantum theory [75], spurring extensive investigations into fundamental problems such as a dynamical metric [76] and dissipative quantum chaos [77] across a broad range of physics. The novel critical phenomenon in the NQKR system might serve as a new element in the field of non-Hermitian chaos [73].

III. THEORETICAL ANALYSIS

As an illustration, we provide detailed derivations of C_f below. (See Appendixes A and B for a detailed derivation of C_p.) It is straightforward to obtain the relation

$$C_f(t) = C_1(t) + C_2(t) - 2\mathrm{Re}[C_3(t)], \tag{6}$$

where the two-point correlators are defined as

$$C_1(t) := \langle A^\dagger(t)B^2A(t)\rangle = \langle \psi_R(t_0)|B^2|\psi_R(t_0)\rangle, \tag{7}$$

$$C_2(t) := \langle B^\dagger A^\dagger(t)A(t)B\rangle = \langle \varphi_R(t_0)|\varphi_R(t_0)\rangle, \tag{8}$$

and the four-point correlator

$$C_3(t) := \langle A^\dagger(t)BA(t)B\rangle = \langle \psi_R(t_0)|B|\varphi_R(t_0)\rangle. \tag{9}$$

Here, $|\psi_R(t_0)\rangle = U^\dagger(t)AU(t)|\psi(t_0)\rangle$ and $|\varphi_R(t_0)\rangle = U^\dagger(t)AU(t)B|\psi(t_0)\rangle$ represent the states at the end of time reversal.

Given $A = e^{i\varepsilon p}$ and $B = |\psi(t_0)\rangle\langle\psi(t_0)|$, we obtain the equivalences $C_1(t) = C_3(t) = |\langle\psi(t)|e^{i\varepsilon p}|\psi(t)\rangle|^2$ and $C_2(t) = \langle\psi(t)|e^{-i\varepsilon p}U(t)U^\dagger(t)e^{i\varepsilon p}|\psi(t)\rangle = |\langle\psi(t)|\psi(t)\rangle|^2$. Consequently, $C_f(t) = |\langle\psi(t)|\psi(t)\rangle|^2 - |\langle\psi(t)|e^{i\varepsilon p}|\psi(t)\rangle|^2$, with the latter term referred to as fidelity out-of-time-ordered correlators (FOTOCs), i.e., $\mathcal{F}_o = |\langle\psi(t)|e^{i\varepsilon p}|\psi(t)\rangle|^2$ [59–61]. It should be noted that the norm $\mathcal{N}(t) = \langle\psi(t)|\psi(t)\rangle$ of non-Hermitian systems unboundedly increases for sufficiently large non-Hermitian parameters. To remove the influence of the norm, we define the rescaled FOTOCs as $\mathcal{F}_o(t) = |\langle\psi(t)|e^{i\varepsilon p}|\psi(t)\rangle/\mathcal{N}(t)|^2$, thus yielding $C_f(t) = 1 - \mathcal{F}_o(t)$. Considering the approximation $e^{i\varepsilon p} \approx 1 + i\varepsilon p$ for $\varepsilon \ll 1$, the FOTOCs can be described as $\mathcal{F}_o(t) \approx 1 - \varepsilon^2[\langle\psi(t)|p^2|\psi(t)\rangle - \langle\psi(t)|p|\psi(t)\rangle^2]$. Therefore, we have

$$C_f(t) \approx \varepsilon^2[\langle\psi(t)|p^2|\psi(t)\rangle - \langle\psi(t)|p|\psi(t)\rangle^2]. \tag{10}$$

In the main quantum resonance condition $\hbar_{\mathrm{eff}} = 4\pi$, each matrix element of U_f equals unity, i.e., $U_f(n) = \exp(-in^2\hbar/2) = 1$, rendering it ineffective in the time evolution of quantum states. The quantum state at any given time t can be obtained by multiplying the initial state with the kicking evolution operator t times, i.e., $|\psi(t)\rangle = U_K^t|\psi(t_0)\rangle$. By setting the ground state as the initial state [i.e., $\psi(t_0) = 1/\sqrt{2\pi}$], the quantum state $|\psi(t)\rangle$ in coordinate space takes the form

$$\psi(\theta, t) = \frac{1}{\sqrt{2\pi}} \exp\left\{-\frac{it}{4\pi}[(K + i\lambda)\cos(\theta)]\right\}, \tag{11}$$

where the norm $\mathcal{N}(t) = I_0(\lambda t/2\pi)$, and $I_m(x)$ denotes the modified Bessel function of order m (see Appendix B). It is worth noting that, for $\lambda t/2\pi \gg 1$, the norm $\mathcal{N}(t) \approx \exp(\lambda t/2\pi)/\sqrt{\lambda t}$ increases unboundedly with time even for arbitrarily small λ, indicating that the quasienergies are complex in the quantum resonance case [74].

The even symmetry of the state in Eq. (11) results in zero mean momentum, i.e., $\langle p(t)\rangle = 0$. Lengthy but straightforward derivations yield the rescaled mean square of momentum by dividing the norm

$$\langle p^2(t)\rangle = 2\pi t \frac{I_1\left(\frac{\lambda t}{2\pi}\right)}{I_0\left(\frac{\lambda t}{2\pi}\right)} \frac{K^2 + \lambda^2}{\lambda}. \tag{12}$$

Combining Eqs. (12) and (10), we obtain the relation

$$C_f(t) \approx 2\pi\varepsilon^2 t \frac{I_1\left(\frac{\lambda t}{2\pi}\right)}{I_0\left(\frac{\lambda t}{2\pi}\right)} \frac{K^2 + \lambda^2}{\lambda}. \tag{13}$$

Consider two limits: $\lambda t/2\pi \ll 1$ and $\lambda t/2\pi \gg 1$. In the $\lambda t/2\pi \ll 1$ limit, where $\lambda \ll 1$ and $t \ll 1/\lambda$, we can make the estimations

$$I_1\left(\frac{\lambda t}{2\pi}\right) \approx \frac{1}{\Gamma(2)}\frac{\lambda t}{4\pi} = \frac{\lambda t}{4\pi} \quad \text{and} \quad I_0\left(\frac{\lambda t}{2\pi}\right) \approx \frac{1}{\Gamma(1)} = 1, \tag{14}$$

where $\Gamma(x)$ is the Gamma function, with $\Gamma(2) = 1$ and $\Gamma(1) = 1$. Thus, C_f can be approximated as

$$C_f(t) \approx \frac{\varepsilon^2 K^2 t^2}{2} \quad \text{with} \quad \lambda = 0. \tag{15}$$

For $\frac{\lambda t}{2\pi} \gg 1$, the relation $I_0(\frac{\lambda t}{2\pi}) \approx I_1(\frac{\lambda t}{2\pi})$ yields

$$C_f(t) \approx 2\pi\varepsilon^2 t \frac{K^2 + \lambda^2}{\lambda}. \tag{16}$$

Both Eqs. (15) and (16) have been summarized in Eq. (3).

IV. CONCLUSION AND DISCUSSIONS

In this work, we investigate the dynamics of various OTOCs, including the FOTOCs, via a NQKR model with the quantum resonance condition. Analytical functions of the OTOCs on both the system parameters and time are achieved and confirmed by our numerical results as well. They demonstrate the linear growth of various OTOCs with time in the non-Hermitian regime, with a remarkable divergence of the growth rate at the zero value of the imaginary part of the kicking potential. This unveils the existence of a Floquet-driving-induced quantum criticality at the boundary between the Hermitian and non-Hermitian regimes. In recent years, the rich physics exhibited by Floquet systems has attracted increasing attention, which spurs potential applications of Floquet engineering, such as manipulating the Anderson metal-insulator transition [78,79], many-body dynamical localization [80–82], and topological phases [83–93]. In this context, our findings represent a significant advancement in exploring novel phases within non-Hermitian Floquet systems [94]. Given that the FOTOCs is directly proportional to the QFI [62], the divergence of the FOTOCs at $\lambda = 0$ holds practical significance in enhancing the measurement precision of quantum sensing [63,95–97].

Based on the mathematical equivalence between the propagation equation of light under paraxial approximations and the Schrödinger equation [98], quantum simulation using optical setups has become an active field for experimentally confirming fundamental concepts of quantum mechanics, including topologically protected transport [99–102], Anderson localization [103–105], and Bloch oscillations [106,107]. The paradigmatic kicked rotor model has been realized using all-optical systems, where the periodically modulated refractive index of optical fibers [108,109] or the periodically arranged phase gratings with equal distance [110,111] mimic the delta-kicking potential for a quantum particle. The well-known dynamical localization of light in the frequency domain has been observed. Notably, the quantum resonance condition can

be achieved by tuning the distance between phase gratings, allowing for experimental realizations of both ballistic diffusion and ratchet transport in momentum space [112]. It is worth noting that the loss feature of phase gratings has been utilized to emulate the $\mathcal{PT}$-symmetric kicked rotor model [74]. Therefore, the NQKR model is achievable in state-of-the-art optical experiments, in which the FOTOCs, proportional to the mean energy, can be measured in the frequency domain.

ACKNOWLEDGMENTS

W.-L.Z. is supported by the National Natural Science Foundation of China (Grants No. 12065009 and No. 12365002), the Natural Science Foundation of Jiangxi province (Grants No. 20224ACB201006 and No. 20224BAB201023), and the Science and Technology Planning Project of Ganzhou City (Grant No. 202101095077). J.L. is supported by the NSAF (Contract No. U2330401).

APPENDIX A: NUMERICAL METHOD FOR CALCULATING OTOCs

The OTOCs are defined as $C(t) = -\langle|[A(t), B]|^2\rangle$ with $A(t) = U^\dagger(t)AU(t)$ [54–57]. The decomposition of OTOCs can be expressed as

$$C(t) = C_1(t) + C_2(t) - 2\mathrm{Re}[C_3(t)], \tag{A1}$$

with

$$C_1(t) := \langle A^\dagger(t)B^2A(t)\rangle = \langle\psi_R(t_0)|B^2|\psi_R(t_0)\rangle, \tag{A2}$$

$$C_2(t) := \langle B^\dagger A^\dagger(t)A(t)B\rangle = \langle\varphi_R(t_0)|\varphi_R(t_0)\rangle, \tag{A3}$$

and

$$C_3(t) := \langle A^\dagger(t)BA(t)B\rangle = \langle\psi_R(t_0)|B|\varphi_R(t_0)\rangle, \tag{A4}$$

where $|\psi_R(t_0)\rangle = U^\dagger(t)AU(t)|\psi(t_0)\rangle$ and $|\varphi_R(t_0)\rangle = U^\dagger(t)AU(t)B|\psi(t_0)\rangle$ represent the states at the end of time reversal [58].

There are four steps for calculating C_1 for a specific time $t = t_n$:

(i) At the initial time $t = t_0$, we choose an initial state $|\psi(t_0)\rangle$ with a unity norm $\mathcal{N}_\psi(t_0) = \langle\psi(t_0)|\psi(t_0)\rangle = 1$.

(ii) From $t = t_0$ to $t = t_n$, forward time evolution yields the state

$$|\psi(t_n)\rangle = U(t_n)|\psi(t_0)\rangle, \tag{A5}$$

with the norm $\mathcal{N}_\psi(t_n) = \langle\psi(t_n)|\psi(t_n)\rangle$. Nonunitary evolution of non-Hermitian systems leads to the growth of the norm, i.e., $\mathcal{N}_\psi(t_n) > \mathcal{N}_\psi(t_0)$. Accordingly, we use the ratio $\mathcal{F}_\psi = \mathcal{N}_\psi(t_n)/\mathcal{N}_\psi(t_0)$ to measure the increase in the norm.

(iii) At time $t = t_n$, we apply the operator A to the state $|\psi(t_n)\rangle$,

$$|\tilde{\psi}(t_n)\rangle = A|\psi(t_n)\rangle, \tag{A6}$$

with the norm $\tilde{\mathcal{N}}_\psi(t_n) = \langle\tilde{\psi}(t_n)|\tilde{\psi}(t_n)\rangle = \langle\psi(t_n)|A^2|\psi(t_n)\rangle$, which is the expectation value of the operator A^2.

(iv) From $t = t_n$ to $t = t_0$, backward evolution (i.e., time reversal) starting from the state $|\tilde{\psi}(t_n)\rangle$ yields

$$|\psi_R(t_0)\rangle = U^\dagger(t_n)|\tilde{\psi}(t_n)\rangle, \tag{A7}$$

with the norm $\mathcal{N}_{\psi_R}(t_0) = \langle\psi_R(t_0)|\psi_R(t_0)\rangle$. Similar to step (ii), we define the factor $\mathcal{F}_{\psi_R} = \mathcal{N}_{\psi_R}(t_0)/\tilde{\mathcal{N}}_\psi(t_n)$ to quantify the growth of the norm.

Since the contribution of the norm to OTOCs is physically meaningless, we define the scaled $C_1(t_n)$ as

$$C_1(t_n) = \frac{C_1(t_n)}{\mathcal{F}_\psi\mathcal{F}_{\psi_R}} = \frac{\langle\psi_R(t_0)|B^2|\psi_R(t_0)\rangle\tilde{\mathcal{N}}_\psi(t_n)}{\mathcal{N}_\psi(t_n)\mathcal{N}_{\psi_R}(t_0)}. \tag{A8}$$

This scaling eliminates the growth of the norm during both the forward and backward evolution. In the above equation, we used the relations $\mathcal{N}_\psi(t_0) = 1$.

Four steps are involved in calculating C_2 at a specific time $t = t_n$:

(i) At $t = t_0$, the initial state $|\varphi(t_0)\rangle = B|\psi(t_0)\rangle$ is obtained, with a norm $\mathcal{N}_\varphi(t_0) = \langle\psi(t_0)|B^2|\psi(t_0)\rangle$, which is the expectation value of B^2 over $|\psi(t_0)\rangle$.

(ii) From t_0 to t_n, forward time evolution yields $|\varphi(t_n)\rangle = U(t_n)|\varphi(t_0)\rangle$ with a norm $N_\varphi(t_n) = \langle\varphi(t_n)|\varphi(t_n)\rangle$. Similar to step (ii) of $C_1(t_n)$, we define a factor $\mathcal{F}_\varphi = \mathcal{N}_\varphi(t_n)/\mathcal{N}_\varphi(t_0)$ to measure the norm increase.

(iii) At $t = t_n$, we apply the operator A to $|\varphi(t_n)\rangle$,

$$|\tilde{\varphi}(t_n)\rangle = A|\varphi(t_n)\rangle, \tag{A9}$$

with the norm $\tilde{\mathcal{N}}_\varphi(t_n) = \langle\tilde{\varphi}(t_n)|\tilde{\varphi}(t_n)\rangle = \langle\varphi(t_n)|A^2|\varphi(t_n)\rangle$.

(iv) For $t_n \to t_0$, the backward evolution is performed by

$$|\varphi_R(t_0)\rangle = U^\dagger(t_n)|\tilde{\varphi}(t_n)\rangle, \tag{A10}$$

with a norm $N_{\varphi_R}(t_0) = \langle\varphi_R(t_0)|\varphi_R(t_0)\rangle$. We use the ratio $\mathcal{F}_{\varphi_R} = \mathcal{N}_{\varphi_R}(t_0)/\tilde{\mathcal{N}}_\varphi(t_n)$ to quantify the norm growth during time reversal.

Similar to the scaling of $C_1(t_n)$, we define the rescaled $C_2(t_n)$ as

$$\begin{aligned} C_2(t_n) &= \frac{C_2(t_n)}{\mathcal{F}_\varphi\mathcal{F}_{\varphi_R}} \\ &= \langle\varphi_R(t_0)|\varphi_R(t_0)\rangle\frac{\mathcal{N}_\varphi(t_0)\tilde{\mathcal{N}}_\varphi(t_n)}{\mathcal{N}_\varphi(t_n)\mathcal{N}_{\varphi_R}(t_0)} \\ &= \frac{\mathcal{N}_\varphi(t_0)}{\mathcal{N}_\varphi(t_n)}\tilde{\mathcal{N}}_\varphi(t_n). \end{aligned} \tag{A11}$$

Given the availability of both $|\psi_R(t_0)\rangle$ and $|\varphi_R(t_0)\rangle$, we can define the rescaled $C_3(t_n)$ as

$$\begin{aligned} C_3(t_n) &= \frac{C_3(t_n)}{\sqrt{\mathcal{F}_\psi\mathcal{F}_{\psi_R}\mathcal{F}_\varphi\mathcal{F}_{\varphi_R}}} \\ &= \langle\psi_R(t_0)|B|\varphi_R(t_0)\rangle\sqrt{\frac{\tilde{\mathcal{N}}_\psi(t_n)}{\mathcal{N}_\psi(t_n)\mathcal{N}_{\psi_R}(t_0)}} \\ &\quad\times\sqrt{\frac{\mathcal{N}_\varphi(t_0)\tilde{\mathcal{N}}_\varphi(t_n)}{\mathcal{N}_\varphi(t_n)\mathcal{N}_{\varphi_R}(t_0)}}, \end{aligned} \tag{A12}$$

where we have used the relation $\mathcal{N}_\psi(t_0) = 1$.

APPENDIX B: THE OTOCs OF A NON-HERMITIAN KICKED ROTOR WITH RESONANCE

The Hamiltonian of NQKR reads

$$\mathrm{H} = \frac{p^2}{2} + (K + i\lambda)\cos(\theta)\sum_n \delta(t - t_n), \tag{B1}$$

where $p = -i\hbar_{\mathrm{eff}}\partial/\partial\theta$ is the angular momentum operator, θ is the angle coordinate, $\hbar_{\mathrm{eff}}$ is the effective Planck constant, K denotes the strength of the real part of the kicking potential, and λ indicates the strength of its imaginary part [51,52]. All variables are properly scaled, hence in dimensionless units. In the quantum resonance condition $\hbar_{\mathrm{eff}} = 4\pi$, the free evolution operator has no effect on the quantum states, as its matrix elements are equal to unity, i.e., $U_f(n) = \exp(-in^2\hbar_{\mathrm{eff}}/2) = 1$. Therefore, only the kicking evolution, governed by the Floquet operator $U_K(\theta) = \exp[-\frac{i}{4\pi}(K + i\lambda)\cos(\theta)]$, needs to be considered. At an arbitrary time $t = t_n$, the quantum state in coordinate space can be precisely expressed as

$$\begin{aligned}\psi(\theta, t_n) &= U_K^{t_n}(\theta)\psi(\theta, t_0)\\ &= \exp\left[-\frac{i}{4\pi}(K + i\lambda)t_n\cos(\theta)\right]\psi(\theta, t_0).\end{aligned} \tag{B2}$$

The OTOCs, constructed using operators $A = p$ and $B = \theta$, take the form

$$C_p(t_n) = -\langle[p(t_n), \theta]^2\rangle = C_1(t_n) + C_2(t_n) - 2\mathrm{Re}[C_3(t_n)], \tag{B3}$$

with

$$C_1(t_n) = \langle\psi_R(t_0)|\theta^2|\psi_R(t_0)\rangle, \tag{B4}$$

$$C_2(t_n) = \langle\varphi_R(t_0)|\varphi_R(t_0)\rangle, \tag{B5}$$

and

$$C_3(t_n) = \langle\psi_R(t_0)|\theta|\varphi_R(t_0)\rangle. \tag{B6}$$

Both $|\psi_R(t_0)\rangle = U^\dagger(t_n)pU(t_n)|\psi(t_0)\rangle$ and $|\varphi_R(t_0)\rangle = U^\dagger(t_n)pU(t_n)\theta|\psi(t_0)\rangle$ represent the states at the end of time reversal.

1. Detailed derivation of $C_1(t_n)$

For convenience in analytical derivation, we adopt the uniform ground state $\psi(\theta, t_0) = 1/\sqrt{2\pi}$ as the initial state. Based on Eq. (B2), the quantum state can be expressed as

$$\psi(\theta, t_n) = \frac{1}{\sqrt{2\pi}}\exp\left[-\frac{i}{4\pi}(K + i\lambda)t_n\cos(\theta)\right]. \tag{B7}$$

The norm of this state is given by

$$\mathcal{N}_\psi(t_n) = \int_{-\pi}^{\pi} d\theta|\psi(\theta, t_n)|^2 = I_0\left(\frac{\lambda t_n}{2\pi}\right), \tag{B8}$$

where I_0 represents the modified Bessel function of zeroth order. When $\lambda t_n/2\pi \gg 1$, we can approximate the norm as $\mathcal{N}_\psi(t_n) \approx \exp(\lambda t_n/2\pi)/\sqrt{\lambda t_n}$. At time $t = t_n$, applying the operator p to the state $\psi(\theta, t_n)$ gives

$$\tilde{\psi}(\theta, t_n) = p\psi(\theta, t_n) = (K + i\lambda)t_n\sin(\theta)\psi(\theta, t_n), \tag{B9}$$

with the norm

$$\tilde{\mathcal{N}}_\psi(t_n) = \langle\psi(t_n)|p^2|\psi(t_n)\rangle = \frac{2\pi(K^2 + \lambda^2)^2 t_n}{\lambda} I_1\left(\frac{\lambda t_n}{2\pi}\right). \tag{B10}$$

Performing time reversal for $t_n \to t_0$ starting from $\tilde{\psi}(\theta, t_n)$ yields

$$\begin{aligned}\psi_R(\theta, t_0) &= \left[U_K^{t_n}(\theta)\right]^\dagger\tilde{\psi}(\theta, t_n)\\ &= \frac{(K + i\lambda)t_n}{\sqrt{2\pi}}\sin(\theta)\exp\left[\frac{\lambda t_n}{2\pi}\cos(\theta)\right].\end{aligned} \tag{B11}$$

By straightforward calculations, the norm can be obtained as

$$\mathcal{N}_{\psi_R}(t_0) = \int_{-\pi}^{\pi} d\theta|\psi_R(\theta, t_0)|^2 = \frac{(K^2 + \lambda^2)\pi t_n}{\lambda} I_1\left(\frac{\lambda t_n}{\pi}\right). \tag{B12}$$

Based on Eqs. (B4) and (B11), we can derive the expression for $C_1(t_n)$ as follows:

$$\begin{aligned}C_1(t_n) &= \int_{-\pi}^{\pi}\theta^2|\psi_R(\theta, t_0)|^2 d\theta\\ &= \frac{|K_\lambda|^2 t_n^2}{2\pi}\int_{-\pi}^{\pi}\theta^2\sin^2(\theta)\exp\left[\frac{\lambda t_n}{\pi}\cos(\theta)\right]d\theta\\ &\approx 3\pi^2\frac{(K^2 + \lambda^2)}{\lambda^2} I_0\left(\frac{\lambda t_n}{\pi}\right),\end{aligned} \tag{B13}$$

where we have used the approximations $\cos(\theta) \approx 1 - \theta^2/2$ and $\sin^2(\theta) \approx \theta^2$ for $\lambda t_n/\pi \gg 1$. By substituting Eqs. (B8), (B10), (B12), and (B13) into Eq. (A8), we obtain the relation

$$C_1(t_n) = C_1(t_n)\frac{\tilde{\mathcal{N}}_\psi(t_n)}{\mathcal{N}_\psi(t_n)\mathcal{N}_{\psi_R}(t_0)} = 6\pi^2\frac{(K^2 + \lambda^2)}{\lambda^2}. \tag{B14}$$

In the Hermitian case $\lambda = 0$, it is straightforward to achieve

$$\begin{aligned}C_1(t_n) &= \int_{-\pi}^{\pi}\theta^2|\psi_R(\theta, t_0)|^2 d\theta\\ &= \frac{K^2 t_n^2}{2\pi}\int_{-\pi}^{\pi}\theta^2\sin^2(\theta)d\theta = \frac{\pi^2 K^2 t_n^2}{6}.\end{aligned} \tag{B15}$$

2. Detailed derivation of $C_2(t_n)$

The initial state is given by $|\varphi(t_0)\rangle = \theta|\psi(t_0)\rangle = \theta/\sqrt{2\pi}$, with a norm

$$\mathcal{N}_\varphi(t_0) = \int_{-\pi}^{\pi} d\theta|\varphi(\theta, t_0)|^2 = \frac{\pi^2}{3}. \tag{B16}$$

The forward evolution from t_0 to t_n yields the state

$$|\varphi(t_n)\rangle = U_K^{t_n}(\theta)|\varphi(t_0)\rangle = U_K^{t_n}(\theta)\theta|\psi(t_0)\rangle = \theta|\psi(t_n)\rangle. \tag{B17}$$

The corresponding norm can be approximated as

$$\begin{aligned}\mathcal{N}_\varphi(t_n) &= \int_{-\pi}^{\pi} d\theta|\varphi(\theta, t_n)|^2\\ &= \int_{-\pi}^{\pi}\theta^2|\psi(\theta, t_n)|^2 d\theta \approx \frac{2\pi}{\lambda t_n} I_0\left(\frac{\lambda t_n}{2\pi}\right),\end{aligned} \tag{B18}$$

where we have used the relation $\cos(\theta) \approx 1 - \theta^2/2$ for $2\lambda t_n/\hbar_{\mathrm{eff}} \gg 1$. At time t_n, applying the operator p to $\varphi(\theta, t_n)$

gives the state

$$|\tilde{\varphi}(t_n)\rangle = p|\varphi(t_n)\rangle = \theta|\tilde{\psi}(t_n)\rangle - i4\pi|\psi(t_n)\rangle. \quad \text{(B19)}$$

In the condition that $\lambda t_n/2\pi \gg 1$, its norm can be described as

$$\tilde{N}_\varphi(t_n) = \langle\tilde{\varphi}(t_n)|\tilde{\varphi}(t_n)\rangle \approx 12\pi^2\frac{(K^2+\lambda^2)}{\lambda^2}I_0\left(\frac{\lambda t_n}{2\pi}\right). \quad \text{(B20)}$$

For backward evolution from t_n to t_0, starting from the state $|\tilde{\varphi}(t_n)\rangle$ in Eq. (B19), we obtain

$$|\varphi_R(t_0)\rangle = U^\dagger(t_n)|\tilde{\varphi}(t_n)\rangle = \theta|\psi_R(t_0)\rangle - i4\pi|\psi_f(t_0)\rangle, \quad \text{(B21)}$$

with $|\psi_f(t_0)\rangle = [U_K^{t_n}(\theta)]^\dagger|\psi(t_n)\rangle$. Straightforward derivation yields the norm

$$\begin{aligned}\mathcal{N}_{\varphi_R}(t_0) = {}& \langle\psi_R(t_0)|\theta^2|\psi_R(t_0)\rangle + 16\pi^2\langle\psi_f(t_0)|\psi_f(t_0)\rangle \\ & - 8\pi\,\mathrm{Im}[\langle\psi_f(t_0)|\theta|\psi_R(t_0)\rangle], \end{aligned} \quad \text{(B22)}$$

where the Im[·] indicates the imaginary part of a complex variable.

The first term in the right side of Eq. (B22) can be approximated as

$$\begin{aligned}\langle\psi_R(t_0)|\theta^2|\psi_R(t_0)\rangle &= (K^2+\lambda^2)t_n^2\int_{-\pi}^{\pi}\theta^2\sin^2(\theta) \\ &\quad\times\exp\left[\frac{\lambda t_n}{2\pi}\cos(\theta)\right]|\psi(\theta,t_n)|^2 d\theta \\ &\approx 3\pi^2\frac{(K^2+\lambda^2)}{\lambda^2}I_0\left(\frac{\lambda t_n}{\pi}\right). \end{aligned} \quad \text{(B23)}$$

The second term is

$$\begin{aligned}&16\pi^2\langle\psi_f(t_0)|\psi_f(t_0)\rangle \\ &= 16\pi^2\int_{-\pi}^{\pi}\exp\left[\frac{\lambda t_n}{2\pi}\cos(\theta)\right]|\psi(\theta,t_n)|^2 d\theta \\ &= 16\pi^2 I_0\left(\frac{\lambda t_n}{\pi}\right). \end{aligned} \quad \text{(B24)}$$

The third term is

$$\begin{aligned}&8\pi\,\mathrm{Im}[\langle\psi_f(t_0)|\theta|\psi_R(t_0)\rangle] \\ &= 4\lambda t_n\int_{-\pi}^{\pi}\exp\left[\frac{\lambda t_n}{\pi}\cos(\theta)\right]\theta\sin(\theta)d\theta \\ &\approx 8\pi^2 I_0\left(\frac{\lambda t_n}{\pi}\right). \end{aligned} \quad \text{(B25)}$$

Combing Eqs. (B23)–(B25), we obtain the expression of the norm

$$\mathcal{N}_{\varphi_R}(t_0) = \pi^2\frac{3K^2+11\lambda^2}{\lambda^2}I_0\left(\frac{\lambda t_n}{\pi}\right). \quad \text{(B26)}$$

Plugging Eqs. (B16), (B18), and (B20) into Eq. (A11) yields $C_2(t_n)$,

$$C_2(t_n) = \tilde{\mathcal{N}}_\varphi(t_n)\frac{\mathcal{N}_\varphi(t_0)}{\mathcal{N}_\varphi(t_n)} \approx 2\pi^3\frac{(K^2+\lambda^2)}{\lambda}t_n. \quad \text{(B27)}$$

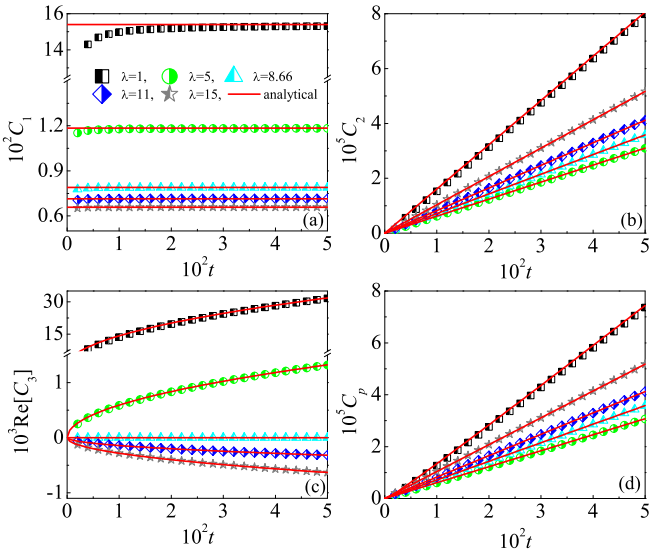

FIG. 3. Time dependence of C_1 (a), C_2 (b), Re[C_3] (c), and C_p (d) with $\lambda = 1$ (squares), 5 (circles), 8.66 (triangles), 11 (diamonds), and 15 (pentagrams). The red lines in (a), (b), (c), and (d) indicate our theoretical prediction in Eqs. (B14), (B27), (B31), and (B33), respectively. The parameters are $K = 5$ and $\hbar_{\mathrm{eff}} = 4\pi$.

In the Hermitian case, i.e., $\lambda = 0$, both $\psi_f(\theta, t_0)$ and $\psi_R(\theta, t_0)$ are real. Therefore, the $C_2(t_n)$ has the expression

$$\begin{aligned}C_2(t_n) &= \langle\psi_R(t_0)|\theta^2|\psi_R(t_0)\rangle + 16\pi^2\langle\psi_f(t_0)|\psi_f(t_0)\rangle \\ &= \frac{\pi^2K^2}{6}t_n^2 + 16\pi^2. \end{aligned} \quad \text{(B28)}$$

3. Detailed derivation of $C_3(t_n)$

The $C_3(t_n)$ is defined as

$$\begin{aligned}C_3(t_n) &= \langle\psi_R(t_0)|\theta|\varphi_R(t_0)\rangle \\ &= \langle\psi_R(t_0)|\theta^2|\psi_R(t_0)\rangle - i4\pi\langle\psi_R(t_0)|\theta|\psi_f(t_0)\rangle. \end{aligned} \quad \text{(B29)}$$

By using Eqs. (B23) and (B25), we can derive its real part,

$$\begin{aligned}\mathrm{Re}[C_3(t_n)] &= \langle\psi_R(t_0)|\theta^2|\psi_R(t_0)\rangle - 4\pi\,\mathrm{Im}[\langle\psi_f(t_0)|\theta|\psi_R(t_0)\rangle] \\ &\approx \pi^2\frac{3K^2-\lambda^2}{\lambda^2}I_0\left(\frac{\lambda t_n}{\pi}\right). \end{aligned} \quad \text{(B30)}$$

Applying Eq. (A12), the rescaled Re[$C_3(t_n)$] can be written as

$$\begin{aligned}\mathrm{Re}[C_3(t_n)] &= \mathrm{Re}[C_3(t_n)]\sqrt{\frac{\mathcal{N}_\psi(t_0)\tilde{\mathcal{N}}_\psi(t_n)}{\mathcal{N}_\psi(t_n)\mathcal{N}_{\psi_R}(t_0)}}\sqrt{\frac{\mathcal{N}_\varphi(t_0)\tilde{\mathcal{N}}_\varphi(t_n)}{\mathcal{N}_\varphi(t_n)\mathcal{N}_{\varphi_R}(t_0)}} \\ &= \frac{\pi^2(3K^2-\lambda^2)}{\lambda^2}\sqrt{\frac{4\pi\lambda(K^2+\lambda^2)}{3K^2+11\lambda^2}}\sqrt{t_n}. \end{aligned} \quad \text{(B31)}$$

In the Hermitian case, $C_3(t_n)$ has the expression

$$\begin{aligned}\mathrm{Re}[C_3(t_n)] &= \langle\psi_R(t_0)|\theta^2|\psi_R(t_0)\rangle \\ &= \frac{K^2}{2\pi}t_n^2\int_{-\pi}^{\pi}\theta^2\sin^2(\theta)d\theta = \frac{\pi^2K^2t_n^2}{6}. \end{aligned} \quad \text{(B32)}$$

Combining Eqs. (B14), (B27), and (B31) yields the expression of the OTOCs for $\lambda t_n \gg 1$,

$$C_p(t_n) = C_1(t_n) + C_2(t_n) - 2\,\mathrm{Re}[C_3(t_n)]$$
$$\approx 2\pi^3 \frac{(K^2+\lambda^2)}{\lambda} t_n, \tag{B33}$$

where we neglect the contributions from both the constant term C_1 and the square root of the t_n term of C_3, as they are significantly smaller than C_2 for $t_n \gg 1$. Based on the relations in Eqs. (B15), (B28), and (B32) in the Hermitian case ($\lambda = 0$), we can conclude that

$$C_p(t_n) = 16\pi^2. \tag{B34}$$

To verify the theoretical analysis above, we numerically investigate the time dependence of C_1, C_2, $\mathrm{Re}[C_3]$, and C_p for different λ. Figure 3(a) demonstrates that C_1 rapidly increases to saturation over time for a nonzero λ (e.g., $\lambda = 1$). Furthermore, the saturation value agrees well with Eq. (B14). In the non-Hermitian case [e.g., $\lambda = 1$ in Fig. 3(b)], C_2 linearly increases with time, following the law described by Eq. (B27) perfectly. Interestingly, our numerical results in Fig. 3(c) demonstrate that $\mathrm{Re}[C_3]$ increases (or decreases) as the square root of t for λ smaller (or larger) than a threshold value of $\lambda_c \approx 8.66$, and it is almost zero when $\lambda = \lambda_c$. The threshold value is determined by Eq. (B31), specifically $3K^2 - \lambda^2 = 0$, which confirms the validity of our theoretical prediction. Additionally, the C_p exhibits linear growth with time for nonzero λ and is approximately equal to C_2, as predicted by Eq. (B33) [see Fig. 3(d)].

[1] J. Cardy, *Scaling and Renormalization in Statistical Physics* (Cambridge University Press, Cambridge, England, 1996).

[2] S. Sachdev, *Quantum Phase Transitions* (Cambridge University Press, Cambridge, England, 2011).

[3] Q. Niu, D. J. Thouless, and Y. S. Wu, Quantized Hall conductance as a topological invariant, Phys. Rev. B **31**, 3372 (1985).

[4] X. Liu, S. Tan, Q. H. Wang, L. W. Zhou, and J. B. Gong, Floquet band engineering with Bloch oscillations, Phys. Rev. B **106**, 224309 (2022).

[5] J. Naji, R. Jafari, L. W. Zhou, and A. Langari, Engineering Floquet dynamical quantum phase transitions, Phys. Rev. B **106**, 094314 (2022).

[6] J. Naji, M. Jafari, R. Jafari, and A. Akbari, Dissipative Floquet quantum dynamical phase transition, Phys. Rev. A **105**, 022220 (2022).

[7] R. Jafari, H. Johannesson, A. Langari, and M. A. Martin-Delgado, Quench dynamics and zero-energy modes: The case of the Creutz model, Phys. Rev. B **99**, 054302 (2019).

[8] K. Yang, L. W. Zhou, W. C. Ma, X. Kong, P. F. Wang, X. Qin, X. Rong, Y. Wang, F. Z. Shi, J. B. Gong, and J. F. Du, Floquet dynamical quantum phase transitions, Phys. Rev. B **100**, 085308 (2019).

[9] V. M. Bastidas, P. Pérez-Fernández, M. Vogl, and T. Brandes, Quantum criticality and dynamical instability in the kicked-top model, Phys. Rev. Lett. **112**, 140408 (2014).

[10] V. M. Bastidas, G. Engelhardt, P. Pérez-Fernández, M. Vogl, and T. Brandes, Critical quasienergy states in driven many-body systems, Phys. Rev. A **90**, 063628 (2014).

[11] I. García-Mata, E. Vergini, and D. A. Wisniacki, Impact of chaos on precursors of quantum criticality, Phys. Rev. E **104**, L062202 (2021).

[12] R. Jafari and H. Johannesson, Loschmidt echo revivals: Critical and noncritical, Phys. Rev. Lett. **118**, 015701 (2017).

[13] L. W. Zhou, Q. H. Wang, H. L. Wang, and J. B. Gong, Dynamical quantum phase transitions in non-Hermitian lattices, Phys. Rev. A **98**, 022129 (2018).

[14] A. Larkin and Y. N. Ovchinnikov, Quasiclassical method in the theory of superconductivity, Sov. Phys. JETP **28**, 1200 (1969).

[15] D. A. Roberts and B. Swingle, Lieb-Robinson bound and the butterfly effect in quantum field theories, Phys. Rev. Lett. **117**, 091602 (2016).

[16] H. Shen, P. F. Zhang, R. H. Fan, and H. Zhai, Out-of-time-order correlation at a quantum phase transition, Phys. Rev. B **96**, 054503 (2017).

[17] R. J. Lewis-Swan, S. R. Muleady, and A. M. Rey, Detecting out-of-time-order correlations via quasiadiabatic echoes as a tool to reveal quantum coherence in equilibrium quantum phase transitions, Phys. Rev. Lett. **125**, 240605 (2020).

[18] C. B. Dağ, K. Sun, and L.-M. Duan, Detection of quantum phases via out-of-time-order correlators, Phys. Rev. Lett. **123**, 140602 (2019).

[19] M. Heyl, F. Pollmann, and B. Dóra, Detecting equilibrium and dynamical quantum phase transitions in Ising chains via out-of-time-ordered correlators, Phys. Rev. Lett. **121**, 016801 (2018).

[20] X. F. Nie, B. B. Wei, X. Chen, Z. Zhang, X. Z. Zhao, C. Qiu, Y. Tian, Y. L. Ji, T. Xin, D. W. Lu, and J. Li, Experimental observation of equilibrium and dynamical quantum phase transitions via out-of-time-ordered correlators, Phys. Rev. Lett. **124**, 250601 (2020).

[21] S. Zamani, R. Jafari, and A. Langari, Out-of-time-order correlations and Floquet dynamical quantum phase transition, Phys. Rev. B **105**, 094304 (2022).

[22] C. B. Dağ, L. M. Duan, and K. Sun, Topologically induced prescrambling and dynamical detection of topological phase transitions at infinite temperature, Phys. Rev. B **101**, 104415 (2020).

[23] Q. Bin, L. L. Wan, F. Nori, Y. Wu, and X. Y. Lü, Out-of-time-order correlation as a witness for topological phase transitions, Phys. Rev. B **107**, L020202 (2023).

[24] Y. Ashida, Z. Gong, and M. Ueda, Non-Hermitian physics, Adv. Phys. **69**, 249 (2020).

[25] N. Hatano and D. R. Nelson, Localization transitions in non-Hermitian quantum mechanics, Phys. Rev. Lett. **77**, 570 (1996).

[26] C. Keller, M. K. Oberthaler, R. Abfalterer, S. Bernet, J. Schmiedmayer, and A. Zeilinger, Tailored complex potentials and Friedel's law in atom optics, Phys. Rev. Lett. **79**, 3327 (1997).

[27] Y. Takasu, T. Yagami, Y. Ashida, R. Hamazaki, Y. Kuno, and Y. Takahashi, PT-symmetric non-Hermitian quantum many-body system using ultracold atoms in an optical lattice with

controlled dissipation, Prog. Theor. Exp. Phys. **2020**, 12A110 (2020).
[28] S. Longhi, Optical realization of relativistic non-Hermitian quantum mechanics, Phys. Rev. Lett. **105**, 013903 (2010).
[29] Q. Lin, T. Y. Li, L. Xiao, K. K. Wang, W. Yi, and P. Xue, Topological phase transitions and mobility edges in non-Hermitian quasicrystals, Phys. Rev. Lett. **129**, 113601 (2022).
[30] S. K. Gupta, Y. Zou, X.-Y. Zhu, M.-H. Lu, L.-J. Zhang, X.-P. Liu, and Y.-F. Chen, Parity-time symmetry in non-Hermitian complex optical media, Adv. Mater. **32**, 1903639 (2020).
[31] A. F. Tzortzakakis, K. G. Makris, A. Szameit, and E. N. Economou, Transport and spectral features in non-Hermitian open systems, Phys. Rev. Res. **3**, 013208 (2021).
[32] F. Minganti, A. Miranowicz, R. W. Chhajlany, I. I. Arkhipov, and F. Nori, Hybrid-Liouvillian formalism connecting exceptional points of non-Hermitian Hamiltonians and Liouvillians via postselection of quantum trajectories, Phys. Rev. A **101**, 062112 (2020).
[33] L. P. Kadanoff and J. Swift, Transport coefficients near the critical point: A master-equation approach, Phys. Rev. **165**, 310 (1968).
[34] S. Pancharatnam, The propagation of light in absorbing biaxial crystals: I. Theoretical, Proc. Indian Acad. Sci. **42**, 86 (1955).
[35] M. Berry, Pancharatnam, virtuoso of the Poincaré sphere: An appreciation, Curr. Sci. **67**, 220 (1994).
[36] M. Berry, Physics of nonhermitian degeneracies, Czech. J. Phys. **54**, 1039 (2004).
[37] M. A. Stephanov, Random matrix model of QCD at finite density and the nature of the quenched limit, Phys. Rev. Lett. **76**, 4472 (1996).
[38] H. Markum, R. Pullirsch, and T. Wettig, Non-Hermitian random matrix theory and lattice QCD with chemical potential, Phys. Rev. Lett. **83**, 484 (1999).
[39] S. Yao and Z. Wang, Edge states and topological invariants of non-Hermitian systems, Phys. Rev. Lett. **121**, 086803 (2018).
[40] W.-T. Xue, Y.-M. Hu, F. Song, and Z. Wang, Non-Hermitian edge burst, Phys. Rev. Lett. **128**, 120401 (2022).
[41] S. Longhi, Non-Hermitian skin effect and self-acceleration, Phys. Rev. B **105**, 245143 (2022).
[42] L. H. Li, C. H. Lee, and J. B. Gong, Topological switch for non-Hermitian skin effect in cold-atom systems with loss, Phys. Rev. Lett. **124**, 250402 (2020).
[43] W. Y. Wang, B. Sun, and J. Liu, Adiabaticity in nonreciprocal Landau-Zener tunneling, Phys. Rev. A **106**, 063708 (2022).
[44] L. Zhai and S. Yin, Out-of-time-ordered correlator in non-Hermitian quantum systems, Phys. Rev. B **102**, 054303 (2020).
[45] W. L. Zhao, R. R. Wang, H. Ke, and J. Liu, Scaling laws of the out-of-time-order correlators at the transition to the spontaneous PT-symmetry breaking in a Floquet system, Phys. Rev. A **107**, 062201 (2023).
[46] W. L. Zhao and R. Wang, Scaling laws of out-of-time-order correlators in a non-Hermitian kicked rotor model, Front. Phys. **11**, 1130225 (2023).
[47] W. L. Zhao, Quantization of out-of-time-ordered correlators in non-Hermitian chaotic systems, Phys. Rev. Res. **4**, 023004 (2022).
[48] S. Bera, K. Y. V. Lokesh, and S. Banerjee, Quantum-to-classical crossover in many-body chaos and scrambling from relaxation in a glass, Phys. Rev. Lett. **128**, 115302 (2022).
[49] S. Shivam, A. De Luca, D. A. Huse, and A. Chan, Many-body quantum chaos and emergence of Ginibre ensemble, Phys. Rev. Lett. **130**, 140403 (2023).
[50] W. L. Zhao and H. Q. Zhang, Dynamical stability in a non-Hermitian kicked rotor model, Symmetry **15**, 113 (2023).
[51] I. I. Satija and A. K. Pattanayak, Non-Hermiticity in a kicked model: Decoherence and the semiclassical limit, Phys. Rev. E **65**, 045205(R) (2002).
[52] L. W. Zhou and J. Pan, Non-Hermitian Floquet topological phases in the double-kicked rotor, Phys. Rev. A **100**, 053608 (2019).
[53] D. O. Chudesnikov and V. P. Yakovlev, Bragg scattering on complex potential and formation of super-narrow momentum distributions of atoms in light fields, Laser Phys. **1**, 110 (1991).
[54] J. Li, R. Fan, H. Wang, B. Ye, B. Zeng, H. Zhai, X. Peng, and J. Du, Measuring out-of-time-order correlators on a nuclear magnetic resonance quantum simulator, Phys. Rev. X **7**, 031011 (2017).
[55] K. Hashimoto, K. Murata, and R. Yoshii, Out-of-time-order correlators in quantum mechanics, Energ. Phys. 10 (2017) 138.
[56] I. García-Mata, M. Saraceno, R. A. Jalabert, A. J. Roncaglia, and D. A. Wisniacki, Chaos signatures in the short and long time behavior of the out-of-time ordered correlator, Phys. Rev. Lett. **121**, 210601 (2018).
[57] M. Zonnios, J. Levinsen, M. M. Parish, F. A. Pollock, and K. Modi, Signatures of quantum chaos in an out-of-time-order tensor, Phys. Rev. Lett. **128**, 150601 (2022).
[58] W. L. Zhao, Y. Hu, Z. Li, and Q. Wang, Super-exponential growth of out-of-time-ordered correlators, Phys. Rev. B **103**, 184311 (2021).
[59] B. Yan, L. Cincio, and W. H. Zurek, Information scrambling and Loschmidt echo, Phys. Rev. Lett. **124**, 160603 (2020).
[60] R. J. Lewis-Swan, A. Safavi-Naini, J. J. Bollinger, and A. M. Rey, Unifying scrambling, thermalization and entanglement through measurement of fidelity out-of-time-order correlators in the Dicke model, Nat. Commun. **10**, 1581 (2019).
[61] W. L. Zhao and J. Liu, Superexponential behaviors of out-of-time ordered correlators and Loschmidt echo in a non-Hermitian interacting system, arXiv:2305.12150.
[62] M. Gärttner, P. Hauke, and A. M. Rey, Relating out-of-time-order correlations to entanglement via multiple-quantum coherences, Phys. Rev. Lett. **120**, 040402 (2018).
[63] S. C. Li, L. Pezzè, and A. Smerzi, Multiparticle entanglement dynamics of quantum chaos in a Bose-Einstein condensate, Phys. Rev. A **103**, 052417 (2021).
[64] T. Macrì, A. Smerzi, and L. Pezzè, Loschmidt echo for quantum metrology, Phys. Rev. A **94**, 010102(R) (2016).
[65] R. Hamazaki, K. Fujimoto, and M. Ueda, Operator noncommutativity and irreversibility in quantum chaos, arXiv:1807.02360.
[66] E. B. Rozenbaum, S. Ganeshan, and V. Galitski, Lyapunov exponent and out-of-time-ordered correlator's growth rate in a chaotic system, Phys. Rev. Lett. **118**, 086801 (2017).
[67] L. D'Alessio and M. Rigol, Long-time behavior of isolated periodically driven interacting lattice systems, Phys. Rev. X **4**, 041048 (2014).

[68] G. Casati, B. V. Chirikov, F. M. Izrailev, and J. Ford, in *Stochastic Behavior in Classical and Quantum Hamiltonian Systems*, edited by G. Casati, and J. Ford, Lecture Notes in Physics Vol. 93 (Springer, Berlin, 1979).

[69] S. Adachi, M. Toda, and K. Ikeda, Potential for mixing in quantum chaos, Phys. Rev. Lett. **61**, 655 (1988).

[70] D. Cohen, Quantum chaos, dynamical correlations, and the effect of noise on localization, Phys. Rev. A **44**, 2292 (1991).

[71] S. Wimberger, I. Guarneri, and S. Fishman, Quantum resonances and decoherence for delta-kicked atoms, Nonlinearity **16**, 1381 (2003).

[72] K. Q. Huang, J. Z. Wang, W. L. Zhao, and J. Liu, Chaotic dynamics of a non-Hermitian kicked particle, J. Phys.: Condens. Matter **33**, 055402 (2021).

[73] C. T. West, T. Kottos, and T. Prosen, $\mathcal{PT}$-Symmetric wave chaos, Phys. Rev. Lett. **104**, 054102 (2010).

[74] S. Longhi, Localization, quantum resonances, and ratchet acceleration in a periodically kicked PT -symmetric quantum rotator, Phys. Rev. A **95**, 012125 (2017).

[75] N. Moiseyev, *Non-Hermitian Quantum Mechanics* (Cambridge University Press, Cambridge, 2011).

[76] K. Sim, N. Defenu, P. Molignini, and R. Chitra, Quantum metric unveils defect freezing in non-Hermitian systems, Phys. Rev. Lett. **131**, 156501 (2023).

[77] J. C. Li, T. Prosen, and A. Chan, Spectral statistics of non-Hermitian matrices and dissipative quantum chaos, Phys. Rev. Lett. **127**, 170602 (2021).

[78] J. Chabé, G. Lemarié, B. Grémaud, D. Delande, P. Szriftgiser, and J. C. Garreau, Experimental observation of the Anderson metal-insulator transition with atomic matter waves, Phys. Rev. Lett. **101**, 255702 (2008).

[79] C. S. Tian, A. Altland, and M. Garst, Theory of the Anderson transition in the quasiperiodic kicked rotor, Phys. Rev. Lett. **107**, 074101 (2011).

[80] T. Nag, S. Roy, A. Dutta, and D. Sen, Dynamical localization in a chain of hard core bosons under periodic driving, Phys. Rev. B **89**, 165425 (2014).

[81] L. Tamang, T. Nag, and T. Biswas, Floquet engineering of low-energy dispersions and dynamical localization in a periodically kicked three-band system, Phys. Rev. B **104**, 174308 (2021).

[82] S. H. Chiew, J. B. Gong, L. Kwek, and C. K. Lee, Stability and dynamics of many-body localized systems coupled to a small bath, Phys. Rev. B **107**, 224202 (2023).

[83] L. W. Zhou and J. B. Gong, Non-Hermitian Floquet topological phases with arbitrarily many real-quasienergy edge states, Phys. Rev. B **98**, 205417 (2018).

[84] L. W. Zhou, D.-J. Zhang, Non-Hermitian floquet topological matter—a review, Entropy **25**, 1401 (2023).

[85] J. P. Dahlhaus, J. M. Edge, J. Tworzydło, and C. W. J. Beenakker, Quantum Hall effect in a one-dimensional dynamical system, Phys. Rev. B **84**, 115133 (2011).

[86] E. P. L. van Nieuwenburg, J. M. Edge, J. P. Dahlhaus, J. Tworzydło, and C. W. J. Beenakker, Metal-topological insulator transition in the quantum kicked rotator with $\mathbb{Z}2$ symmetry, Phys. Rev. B **85**, 165131 (2012).

[87] I. Dana and K. Kubo, Floquet systems with Hall effect: Topological properties and phase transitions, Phys. Rev. B **100**, 045107 (2019).

[88] Z. Y. Cheng, R. W. Bomantara, H. R. Xue, W. W. Zhu, J. B. Gong, and B. L. Zhang, Observation of $\pi/2$ modes in an acoustic Floquet system, Phys. Rev. Lett. **129**, 254301 (2022).

[89] K. Yang, S. Y. Xu, L. W. Zhou, Z. Y. Zhao, T. Y. Xie, Z. Ding, W. C. Ma, J. B. Gong, F. Z. Shi, and J. F. Du, Observation of Floquet topological phases with large Chern numbers, Phys. Rev. B **106**, 184106 (2022).

[90] W. W. Zhu, M. Umer, and J. B. Gong, Floquet higher-order Weyl and nexus semimetals, Phys. Rev. Res. **3**, L032026 (2021).

[91] L. H. Li, C. H. Lee, and J. B. Gong, Realistic Floquet semimetal with exotic topological linkages between arbitrarily many nodal loops, Phys. Rev. Lett. **121**, 036401 (2018).

[92] D. Y. H. Ho and J. B. Gong, Quantized adiabatic transport in momentum space, Phys. Rev. Lett. **109**, 010601 (2012).

[93] L. W. Zhou, Floquet engineering of topological localization transitions and mobility edges in one-dimensional non-Hermitian quasicrystals, Phys. Rev. Res. **3**, 033184 (2021).

[94] H. Y. Wang and W. M. Liu, Tightly bound states in a uniform field with asymmetric tunneling, Phys. Rev. A **106**, 052216 (2022).

[95] Y. Chu, Y. Liu, H. Liu, and J. Cai, Quantum sensing with a single-qubit pseudo-Hermitian system, Phys. Rev. Lett. **124**, 020501 (2020).

[96] J. Wiersig, Sensors operating at exceptional points: General theory, Phys. Rev. A **93**, 033809 (2016).

[97] Z.-P. Liu, J. Zhang, Ş. K. Özdemir, B. Peng, H. Jing, X.-Y. Lü, C.-W. Li, L. Yang, F. Nori, and Y.-X. Liu, Metrology with $\mathcal{PT}$-symmetric cavities: Enhanced sensitivity near the $\mathcal{PT}$-phase transition, Phys. Rev. Lett. **117**, 110802 (2016).

[98] S. Longhi, Quantum-optical analogies using photonic structures, Laser Photon. Rev. **3**, 243 (2009).

[99] T. Ozawa, H. M. Price, A. Amo, N. Goldman, M. Hafezi, L. Lu, M. C. Rechtsman, D. Schuster, J. Simon, O. Zilberberg, and I. Carusotto, Topological photonics, Rev. Mod. Phys. **91**, 015006 (2019).

[100] L. Xiao, T. S. Deng, K. K. Wang, G. Y. Zhu, Z. Wang, W. Yi, and P. Xue, Non-Hermitian bulk-boundary correspondence in quantum dynamics, Nat. Phys. **16**, 761 (2020).

[101] D. Smirnova, D. Leykam, Y. Chong, and Y. Kivshar, Nonlinear topological photonics, Appl. Phys. Rev. **7**, 021306 (2020).

[102] Y. Shen, J. Ji, H.-C. Li, L. Zhang, X. Yu, S.-B. Yan, M. Rasmussen, Q. Shen, D. Madhi, B.-B. Zhou, P. U. Jepsen, and X.-H. Deng, Realization of photonic topological insulators at terahertz frequencies characterized by time-domain spectroscopy, Phys. Rev. Appl. **18**, 064025 (2022).

[103] D. S. Wiersma, P. Bartolini, Ad Lagendijk, and R. Righini, Localization of light in a disordered medium, Nature (London) **390**, 671 (1997).

[104] M. Segev, Y. Silberberg, and D. N. Christodoulides, Anderson localization of light, Nat. Photon. **7**, 197 (2013).

[105] W. Schirmacher, B. Abaie, A. Mafi, G. Ruocco, and M. Leonetti, What is the right theory for Anderson localization of light? An experimental test, Phys. Rev. Lett. **120**, 067401 (2018).

[106] S. Longhi, Optical Bloch oscillations and Zener tunneling with nonclassical light, Phys. Rev. Lett. **101**, 193902 (2008).

[107] R. Sapienza, P. Costantino, D. Wiersma, M. Ghulinyan, C. J. Oton, and L. Pavesi, Optical analogue of electronic Bloch oscillations, Phys. Rev. Lett. **91**, 263902 (2003).

[108] R. E. Prange and S. Fishman, Experimental realizations of kicked quantum chaotic systems, Phys. Rev. Lett. **63**, 704 (1989).

[109] O. Agam, S. Fishman, and R. E. Prange, Experimental realizations of quantum chaos in dielectric waveguides, Phys. Rev. A **45**, 6773 (1992).

[110] B. Fischer, A. Rosen, A. Bekker, and S. Fishman, Experimental observation of localization in the spatial frequency domain of a kicked optical system, Phys. Rev. E **61**, R4694(R) (2000).

[111] A. Rosen, B. Fischer, A. Bekker, and S. Fishman, Optical kicked system exhibiting localization in the spatial frequency domain, J. Opt. Soc. Am. B **17**, 1579 (2000).

[112] C. Zhang, C. F. Li, and G. C. Guo, Experimental demonstration of photonic quantum ratchet, Sci. Bull. **60**, 249 (2015).